Int. J. Electrochem. Sci., 12 **(2017)** 9896 – 9906, doi: 10.20964/2017.10.100

International Journal of
ELECTROCHEMICAL
SCIENCE
www.electrochemsci.org

$Li_4Ti_5O_{12}$ Coating Layer as Li^+ Conductor and Cycle Stabilizer for SnO_2 Anode

Gong Shiding, Zhang Yaoyao, Sun Fang, Zeng Tianbiao, Hu Xuebu[*]

College of Chemistry and Chemical Engineering, Chongqing University of Technology, Chongqing 400054, China
[*]E-mail: xuebu@cqut.edu.cn

Received: 14 April 2017 / *Accepted:* 17 May 2017 / *Published:* 12 September 2017

$Li_4Ti_5O_{12}$ as Li^+ conductor and cycle stabilizer was coated successfully on mesoporous SnO_2 spheres (M-SnO_2) via in-situ synthesis. The structure and morphology of as-prepared samples were characterized by X-ray diffraction (XRD), scanning electron microscopy (SEM) and transmission electron microscopy (TEM). The results indicated that the SnO_2 spheres were coated fully by $Li_4Ti_5O_{12}$ layer, and the $Li_4Ti_5O_{12}$ layer did not change the structure or morphology of M-SnO_2. Electrochemical impedance spectra (EIS) and charge/discharge tests showed that the outer $Li_4Ti_5O_{12}$ coating layer enhanced Li^+ diffusion in SnO_2 anode. The Li^+ diffusion coefficient for S-1 and S-2 reached to 9.87×10^{-13} cm^2 s^{-1} and 1.82×10^{-12} cm^2 s^{-1}, while the value of M-SnO_2 was only 6.36×10^{-13} cm^2 s^{-1}. The cycle stability and rate cycle property of SnO_2-based anode were improved significantly due to promotional role of $Li_4Ti_5O_{12}$ coating layer.

Keywords: SnO_2, $Li_4Ti_5O_{12}$, Li^+ conductor, cycle stabilizer, Li^+ diffusion coefficient

1. INTRODUCTION

Compared to commercial graphite/carbon, SnO_2 has been considered as one of the candidate anode for lithium ion batteries due to its higher theoretical capacity (782 mAh g^{-1}) [1, 2]. However, on the one hand, large volume expansion/contraction occurs during Li^+ insertion/extraction, leading to the electrodes pulverization and cracking [3, 4]. On the other hand, Li^+ diffusion in SnO_2 is difficult, which results in its poor cyclability and rate performance [5]. Nowadays, there are some effective strategies to suppress the volume expansion/contraction, such as synthesizing nanoparticles or core-shell particles, or mixing with conductive carbon materials. Nanoparticles include nanospheres, nanotubes, nanosheets, nanobelts and nanofibers, etc. Core-shell particles include carbon coating and TiO_2 coating, etc. The composites include SnO_2 mixing with graphene, mesoporous carbon,

carbonaceous mesophase spherules, carbon tubes, or carbon fibers. [6-10]. Those strategies have improved the cyclability of SnO_2 anode, but the cyclability especially rate cycle performance can not be improved further due to poor Li^+ diffusion. Therefore, how to construct SnO_2 anode with high rate cyclability becomes important.

In recent years, many Li^+ conductors have been synthesized and studied. The Li^+ conductors are usually inorganic lithium salt, such as Li_7AO_6 (A=Sb, Bi, Ta, Zr), $LiBiO_2$, Li_3BiO_3, Li_3BiO_4, Li_5BiO_5, Li_4SiO_4, $Li_4Ti_5O_{12}$, etc [11-14]. However, not all those inorganic lithium salt are suitable using as Li^+ conductor under room temperature condition, some lithium salt (such as Li_7MO_6) need high temperature to ensure the high Li^+ conduction coefficient. Among the above-mentioned lithium salts, $Li_4Ti_5O_{12}$ is one of the most popular Li^+ conductor due to its "zero strain" and high Li^+ diffusion coefficient. The reported value of Li^+ diffusion coefficient was various, such as Yu-Jun Bai et al. reported the value was 3.38×10^{-15} $cm^2\ s^{-1}$[15] and 3.38×10^{-15} $cm^2\ s^{-11}$ [16], and some reports reported the value was ~2.0×10^{-11} $cm^2\ s^{-1}$ [17-18]. Our previous work studied the Li^+ diffusion coefficient value of carbon coated $Li_4Ti_5O_{12}$ spheres was 8.53×10^{-13} $cm^2\ s^{-1}$ [19]. Although the Li^+ diffusion coefficient value of $Li_4Ti_5O_{12}$ was various, but the various reported values were confirmed that $Li_4Ti_5O_{12}$ is a fast Li^+ conductor. The values were various because the measure conditions were not same. From those reported values and the Li^+ diffusion coefficient of pure SnO_2 (Ref. 19), a conclusion can be obtained that the Li^+ diffusion coefficient of pure $Li_4Ti_5O_{12}$ was two orders of magnitude higher than that of pure SnO_2. In recent years, although some works were reported SnO_2-$Li_4Ti_5O_{12}$ composites, such Han et al. [18] synthesized the anode materials composed of 2D $Li_4Ti_5O_{12}$ nanosheets and 0D SnO_2 nanoparticles, however the composite delivered 140 mAh g^{-1} after 30 cycles at current density of 0.1 mA cm^{-2}. The capacity was low because the 2D $Li_4Ti_5O_{12}$ nanosheets were not coated on SnO_2 nanoparticles. Hao et al. [19] synthesized $Li_4Ti_5O_{12}$-SnO_2 composite via sol-gel and high temperature solid-state methods. Its capacity was lower than 200 mAh g^{-1} at 0.5 mA cm^{-2} after 42 cycles because SnO_2 was simply mixed with $Li_4Ti_5O_{12}$. Similarly, Wang et al. [20] also synthesized $Li_4Ti_5O_{12}$-SnO_2 composite. However, its capacity was low because SnO_2 was simply mixed with $Li_4Ti_5O_{12}$.

For improving the cyclability and rate property of SnO_2 anode, $Li_4Ti_5O_{12}$ coated M-SnO_2 were prepared via simple synthesis strategies. Here, $Li_4Ti_5O_{12}$ layer acts as volume expansion/contraction buffer layer and Li^+ conductor to improve the cyclability and rate property of SnO_2 anode.

2. EXPERIMENTAL

2.1 Sample preparation

The synthesis process of $Li_4Ti_5O_{12}$ coated M-SnO_2 spheres were illustrated in Fig. 1. Firstly, 3.9630 g glucose and 2.8040 g $SnCl_4{\cdot}5H_2O$ was dissolved into mixed solution of 10.0 mL deionized water and 60.0 mL absolute alcohol in a 100 mL Teflon-lined stainless steel autoclave and placed in an oven at 150 ℃ for 12 h. The precipitation was collected by centrifugation and washed with deionized water and ethanol several times after cooling down to room temperature. The slurry was dried in vacuum oven under 60℃.and heated at 500 ℃ under air atmospheres for obtaining M-SnO_2. Next,

0.2958 g M-SnO_2 were dispersed into 15.0 mL absolute alcohol by strong stirring and ultrasonic, then 160 μL heptanoic acid, 300 μL ammonium hydroxide, 300 μL tetrabutyl titanate (S-1**)** or 700 μL tetrabutyl titanate (S-2) were dropped, and kept stirring. After 30 min, 7.0 mL deionized water was poured into above suspension quickly and kept stirring for another 2 h. The white precipitation was poured into a 100 mL Teflon-lined stainless steel autoclave and placed in an oven at 150 ℃ for 12 h. After cooling down, the precipitation was collected by centrifugation and washed with deionized water and ethanol several times, then re-dispersed into mixed solution of 15.0 mL absolute alcohol and 30.0 mL deionized water in a 100 mL Teflon-lined stainless steel autoclave and placed in 160 ℃ for 6 h. The white precipitation was collected by centrifugation and washed with deionized water and ethanol several times, and dried in 60 ℃. Finally, the powder was heated in 500 ℃ under air atmospheres for final product. The sample of pure m-SnO_2 spheres named as S-0.

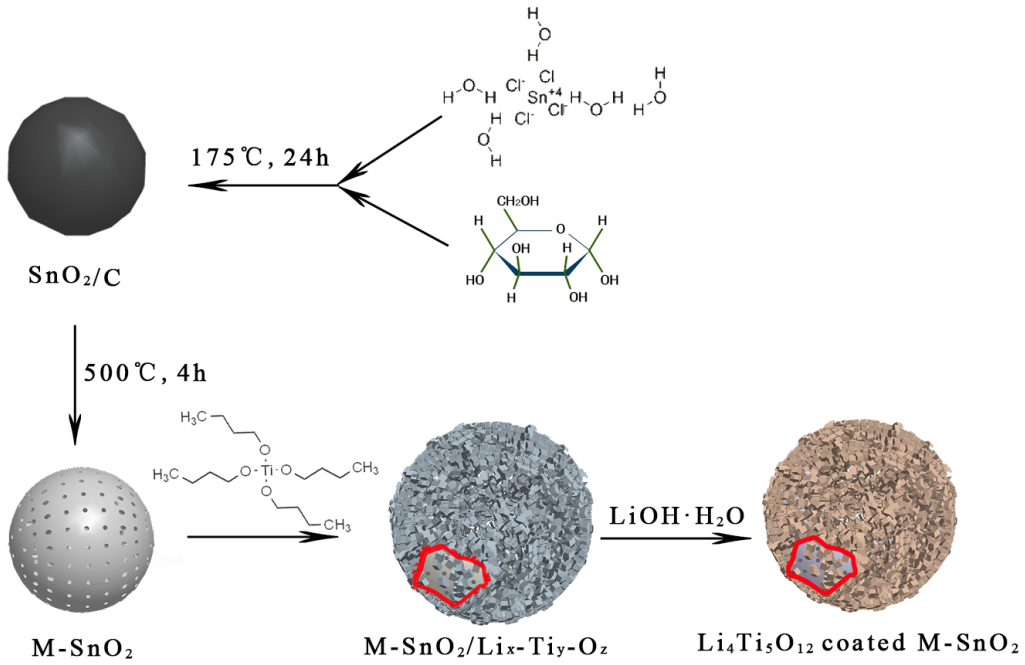

Figure 1. Schematic illustration of the synthesis of $Li_4Ti_5O_{12}$ coated M-SnO_2 spheres. Red circles are cross-section view. From the cross-section view, the inner M-SnO_2 can be seen

2.2 Characterizations

The crystal structure of the samples was studied by XRD (Shimadzu-XRD-7000S, Cu-Kα radiation, λ= 1.54056 Å, 40kV, 40 mA). The morphology was investigated via SEM (S4800) and TEM (FEI Tecnai G20).

2.3 Electrochemical testing

As-prepared samples (80 wt.%), conductive carbon black (10 wt.%) and polyvinylidene fluoride (10 wt.%) binder were mixed using N-methyl pyrrolidine as solvent for homogeneous slurry, then the slurry was pasted uniformly onto a copper foil and dried to give the electrodes with loading

materials of ~2.5 mg cm^{-2}. The CR2032 coin cells were assembled in an argon-filled dry glove box using lithium metal foil as the counter electrode. The electrolyte was 1 $mol \cdot L^{-1}$ $LiPF_6$/(EC+DME+EMC) (1/1/1 by volume) solution. Celgard 2400 polypropylene membrane was used as the separator. Galvanostatic charge/discharge tests were performed on LAND battery tester with a cut-off voltage of 0.01~2.0 V. Electrochemical impedance spectra (EIS) in the frequency range 10^{-2} to 10^5 Hz was performed by an Autolab PGSTAT 128 N electrochemical workstation. Cyclic voltammograms (CV) was acquired in same electrochemical workstation in the voltage range 0 to 3 V.

3. RESULT AND DISCUSSION

3.1 Physical properties

Fig. 2 shows XRD results of the samples. As shown in the figure, the diffraction peaks of S-1 and S-2 were consistent with standard SnO_2 diffraction peaks (JCPDS No: 41-1445) and $Li_4Ti_5O_{12}$ diffraction peaks (JCPDS No: 49-0207), indicating that there was no evidence of impurities. The intensity of $Li_4Ti_5O_{12}$ peaks in S-1 was weaker than that of S-2 due to higher $Li_4Ti_5O_{12}$ content in S-2.

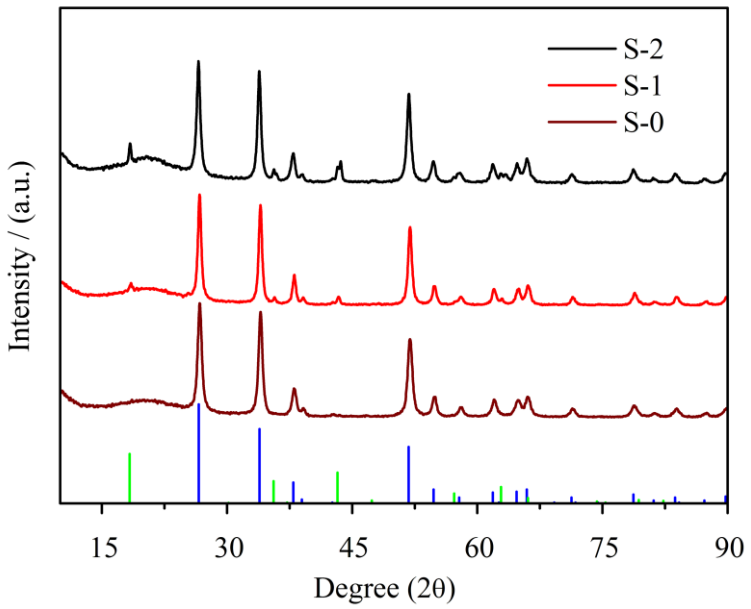

Figure 2. XRD results of S-1 and S-2. The green and blue bars on bottom are standard $Li_4Ti_5O_{12}$ and SnO_2 diffraction peaks

The morphology of the samples was observed via SEM and TEM as shown in Fig. 3. Fig. 3(a) shows that the surface of SnO_2/C spheres was smooth and the spheres particle size was ~1.5 μm. The SnO_2/C spheres were composed of SnO_2 and pyrolytic carbon originated from glucose. Fig. 3(b) shows that there was no mesoporous in surface or inner of SnO_2/C spheres. After SnO_2/C spheres were heated at 500℃ under air atmospheres, the carbon was oxidized and the mesoporous were formed on surface

and inner spheres, as shown in Fig. 3(c)-(d). The mesoporous on the surface was beneficial for adsorbing tetrabutyl titanate molecule due to large specific surface. Fig. 3(e) is the SEM image of S-2. The surface was coarser after $Li_4Ti_5O_{12}$ particles were coated on SnO_2. For unclosing more detail of the $Li_4Ti_5O_{12}$ layer, the sample was observed by TEM. The TEM result was shown in Fig. 3(f)-(i). Fig. 3(f) shows some $Li_4Ti_5O_{12}$ particles were coated on surface. Fig. 3(g) shows the inner mesoporous were not affected after $Li_4Ti_5O_{12}$ layer coated because the mesoporous on the SnO_2 surface has limited the tetrabutyl titanate adsorpted into inner mesoporous. Fig. 3(h) shows the thickness of $Li_4Ti_5O_{12}$ layer was 60~90 nm. Fig. 3(i) discloses the detail of the interface between $Li_4Ti_5O_{12}$ and SnO_2. The lattice fringe of $Li_4Ti_5O_{12}$ was estimated as 0.48 nm, and the lattice fringe of SnO_2 was estimated as 0.26 nm and 0.34 nm. The SEM and TEM results proved that the structure of M-SnO_2 was not affected after $Li_4Ti_5O_{12}$ coating and the structure of final samples was in accordance with the design idea.

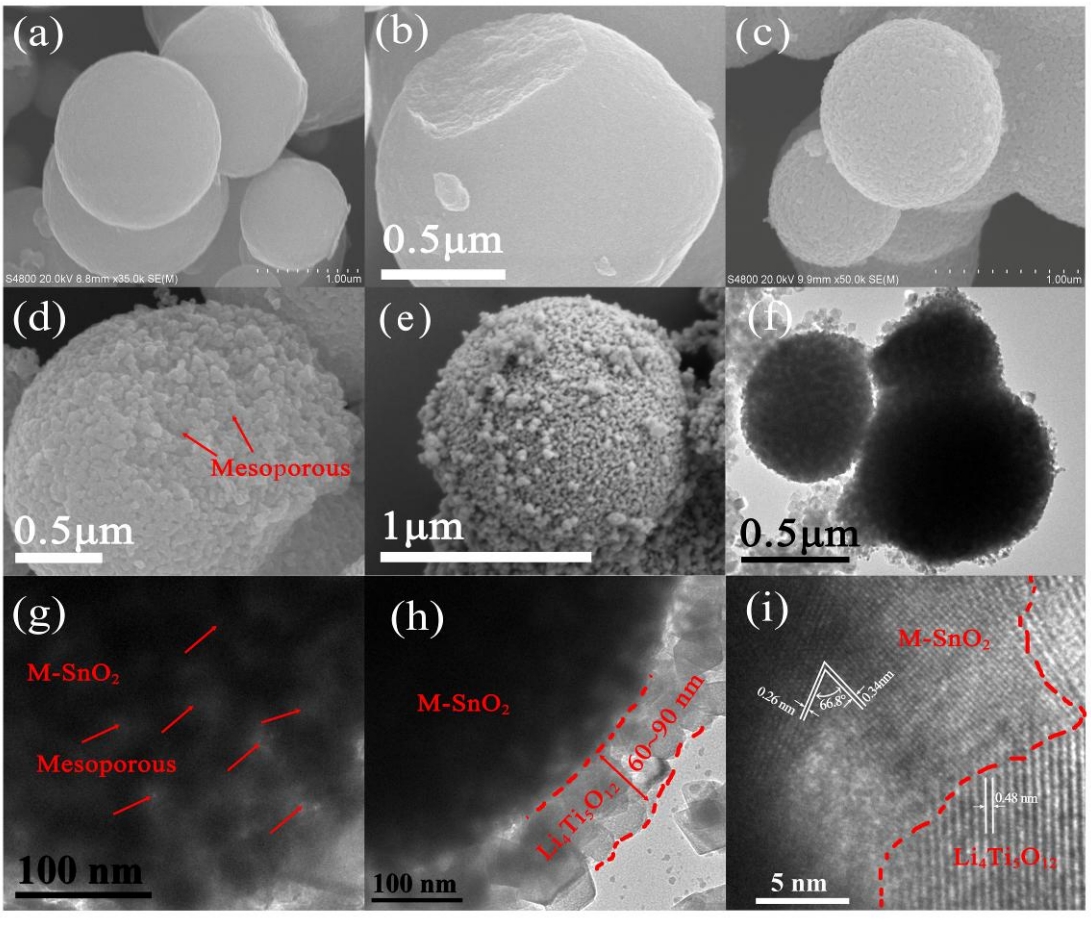

Figure 3. SEM image of SnO_2/C spheres (a, b), M-SnO_2 (c, d), S-2 (e), TEM images of S-2 (f-i)

3.2 Electrochemical performances

The Li^+ diffusion coefficient of the samples was investigated using EIS. Besides S-0, S-1 and S-2, pure $Li_4Ti_5O_{12}$ was also investigated. Fig. 4(a) shows the EIS results. All the EIS curves were

made of a semicircle which located at high frequent and a line which located at low frequent. The larger the semicircle radius, the poorer the electronic conductivity of the samples [21, 22]. In high frequency, the radius of $Li_4Ti_5O_{12}$ was smallest, the radius of S-2 was smaller than that of S-1, and the radius of S-0 was largest, indicating that the electronic conductivity of $Li_4Ti_5O_{12}$ is obviously higher than that of SnO_2. Why? Because the band gap of $Li_4Ti_5O_{12}$ is 2.3 eV [23], while the value of SnO_2 is 3.5 eV [24]. The higher the band gap, the more difficult the electron transition between valence band and conduction band. It is well-known that the higher the band gap, the poorer the electronic conductivity of the materials. For calculating the Li^+ diffusion coefficient, -Z' against $\omega^{1/2}$ was depicted in Fig. 4(b). Li^+ diffusion can be calculated from following equation [17, 25]:

$$D_{Li} = \frac{R^2T^2}{2A^2n^4F^4C_{Li}^2\sigma^2}$$

where *R* is the gas constant (8.3145 J mol^{-1} K^{-1}), *T* is the absolute temperature (298 K), *A* is the area of electrode (1.539 cm^2), *n* is the number of transferred electrons (4.4), *F* is the Faraday constant (96485.6 C mol^{-1}), C_{Li+} is the lithium-ion concentration (0.001 moL cm^{-3}), and σ is the coefficient of Warburg impedance, which is the slope of Z'/-$\omega^{1/2}$ line. D_{Li+} for S-0, S-1 S-2 and pure $Li_4Ti_5O_{12}$ was calculated as 6.36×10^{-13}, 9.87×10^{-13}, 1.82×10^{-12} and 8.89×10^{-11} cm^2 s^{-1}. The Li^+ diffusion coefficient of pure $Li_4Ti_5O_{12}$ here was two orders of magnitude higher than that of M-SnO_2 spheres, which was consistent with the reported results [5, 15-17]. These results show D_{Li+} of SnO_2 material can be increased substantially by $Li_4Ti_5O_{12}$ coating.

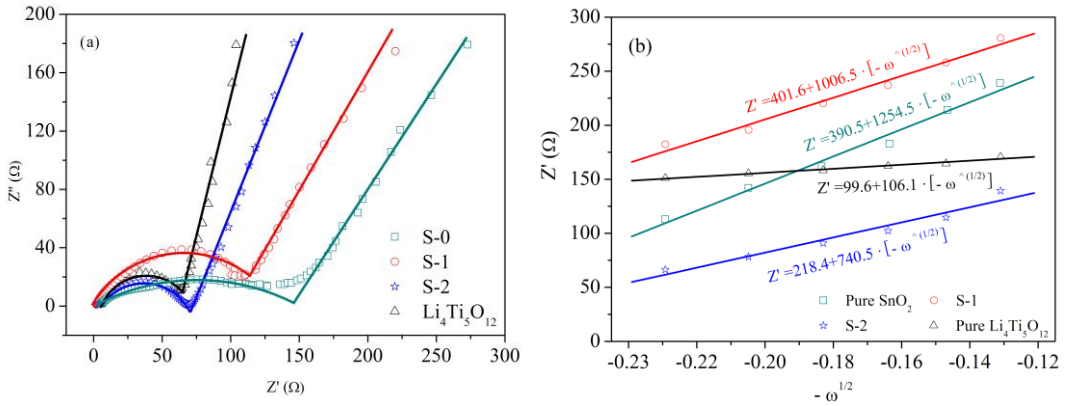

Figure 4. EIS (a) and Z'/-$\omega^{1/2}$ line (b) of S-0, S-1, S-2 and pure $Li_4Ti_5O_{12}$. Dots were experimental data, lines were fitting from dots

Another function of $Li_4Ti_5O_{12}$ layer is as volume expansion/contraction buffer layer to improve the cycle stability, which can be estimated by galvanostatic charge/discharge cycles. Fig. 5(a) shows the results. As shown in the figure, S-2 was more stable than S-1 and S-0 in 50 mA g^{-1} or in 500 mA g^{-1}, indicating that $Li_4Ti_5O_{12}$ coating layer can improve the cyclability of SnO_2. The initial capacity of S-2, S-1 and S-0 at 50 mA g^{-1} was 969.3 mAh g^{-1}, 919.6 mAh g^{-1} and 841.4 mAh g^{-1}, respectively. When the current density was switched to 500 mA g^{-1}, their initial capacity were 731.4 mAh g^{-1}, 822.3 mAh g^{-1} and 542.6 mAh g^{-1}, respectively. At 50 mA g^{-1}after 20 cycles, S-2 and S-1 became stable, while S-0

was not yet. At 100th cycle, the capacity of S-2, S-1 and S-0 was 282.3, 193.3 and 123.9 mAh g^{-1}. The capacity of S-2 and S-1 was 127.8% and 56.1% higher than that of S-0. At 500 mA g^{-1} after 15 cycles, the capacity of S-1 and S-0 still declined fast compared to that of S-2, suggesting that the volume expansion/contraction of S-1 and S-0 were severer than that of S-2. S-2 was more stable because the $Li_4Ti_5O_{12}$ layer was thicker and can relieve the stress of volume expansion/contraction more effectively. For coulombic efficiency, the initial cycle value for S-0 at 50 mA g^{-1} and 500 mA g^{-1} was 39.7% and 37.3%, and the value for S-1 was 46.1% and 47.9%, while the value for S-2 was 48.4% and 42.5%, respectively. Those values were lower than 50%. The reason why those values were lower than 50% was determined by the charge/discharge mechanism of SnO_2, which a conversion reaction was occurred in initial discharged. The initial discharge process of SnO_2 can be described by follow equation [26-29]:

$$SnO_2+8.4Li \rightarrow Li_{4.4}Sn+2Li_2O \quad (1)$$

After the initial discharged, the reaction was as follow:

$$Li_{4.4}Sn \rightleftharpoons 4.4Li+Sn \quad (2)$$

The equation (1) was irreversible, while equation (2) was reversible. From equation (1) and (2), there was 4.4 Li reversible, while there was 8.4 Li reacted with per SnO_2 in initial discharged. Thus, the theoretical coulombic efficiency of initial cycle was 52.38% (4.4/8.4×100%=52.38%) for pure SnO_2. The initial coulombic efficiency was lower than 50% was own to form a SEI film. After the initial cycle, the coulombic efficiency was increase gradually, indicating that the electrodes were become more reversible. However, the increase rate in first 20 cycles was different on S-0, S-1 and S-2 because their $Li_4Ti_5O_{12}$ content was different. It can see that more $Li_4Ti_5O_{12}$ content in electrodes, higher the increase rate of coulombic efficiency in first 20 cycles. The result was suggesting that $Li_4Ti_5O_{12}$ can increase the utilization rate of the SnO_2-based materials. Moreover, the rate cycles can prove the promotional effect of $Li_4Ti_5O_{12}$ layer on SnO_2 anode as well. Fig. 5(b) shows the rate cycles of the samples. At initial five cycles, the capacity of S-2, S-1 and S-0 was approximately equal. The capacity of S-0, S-1 and S-2 at 5th cycle was 706.5, 641.0 and 604.3 mAh g^{-1}, respectively. However, the capacity decline rate of S-1 and S-0 was more and more severe with the increase of the current density. At 10th (100 mA g^{-1}), 15th (200 mA g^{-1}), 20th (500 mA g^{-1}) and 25th (1000 mA g^{-1}) cycle, the discharge capacity of S-2 was 493.9, 351.9, 263.8 and 170.7 mAh g^{-1}, while the value of S-1 was 371.6, 289.6, 184.5 and 110.3 mAh g^{-1}, and the value of S-0 was only 314.5, 242.5, 109.4 and 35.0 mAh g^{-1}. The above values were indicating that S-1 and S-0 were less stable than S-2. Moreover, when the current density was switched from 500 mA g^{-1} to 50 mA g^{-1}, the capacity recovery rate of S-2 was obviously higher than S-1 and S-0, which also proved that S-2 was more stable than S-1 and S-0. The above results proved that $Li_4Ti_5O_{12}$ coating layer played a promotional role on cyclability and rate cycle performance for SnO_2 anode.

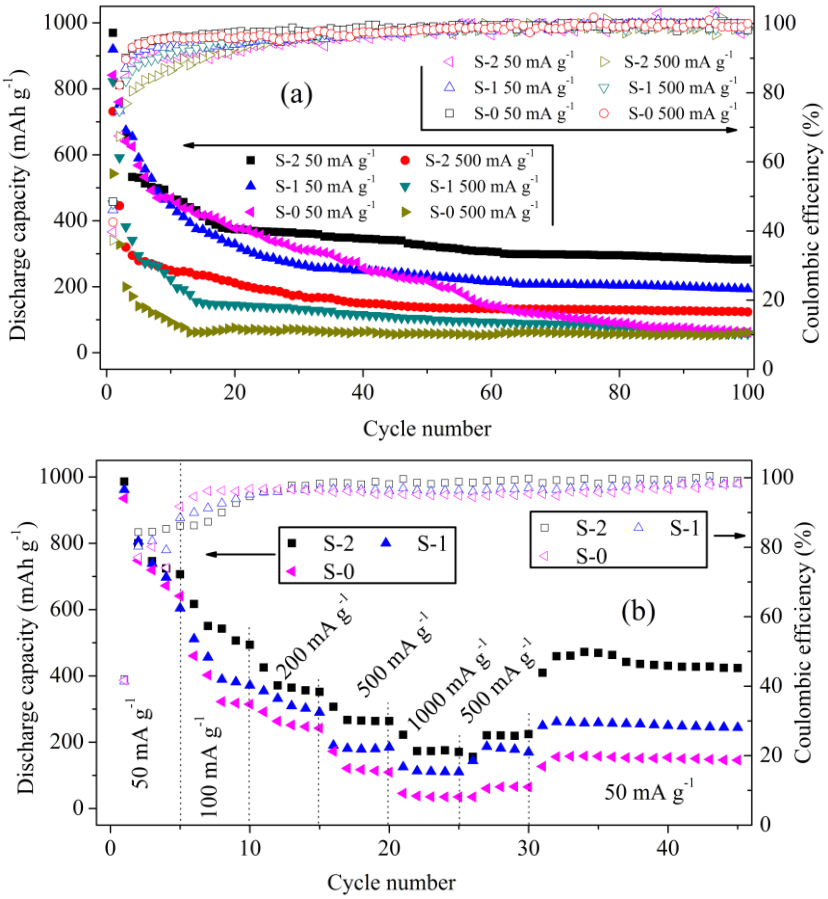

Figure 5. Galvanostatic charge/discharge cycles (a) and rate cycles (b)

The lithiation/delithiation details of the samples were investigated by CVs. Fig. 6(a)~(c) show the CVs results. In first scan of S-2, four pairs peaks denoted as Ⅰ/Ⅰ', Ⅱ/Ⅱ', Ⅲ/Ⅲ' and Ⅳ/Ⅳ' were observed. The peaks of Ⅳ/Ⅳ' were owing to lithiation/delithiation between Li^+ and $Li_4Ti_5O_{12}$, and the peaks of Ⅰ/Ⅰ', Ⅱ/Ⅱ' and Ⅲ/Ⅲ' were owing to lithiation/delithiation between Li^+ and SnO_2. The reaction equations of those peaks were as follows [26-29]:

Peak Ⅳ/Ⅳ': $Li_4Ti_5O_{12}+3Li \Leftrightarrow Li_7Ti_5O_{12}$ (3)

Peak Ⅲ/Ⅲ': $Li+Sn \Leftrightarrow LiSn$ (4)

Peak Ⅱ/Ⅱ': $2LiSn+5Li \Leftrightarrow Li_7Sn_2$ (5)

Peak Ⅰ/Ⅰ': $Li_7Sn_2+1.8Li \Leftrightarrow 2Li_{4.4}Sn$ (6)

Besides peaks of Ⅰ/Ⅰ', Ⅱ/Ⅱ', Ⅲ/Ⅲ' and Ⅳ/Ⅳ', two cathodic peaks denoted as A and B were also observed. The reaction of A peak was as follows [30]:

A: $SnO_2+4Li \rightarrow Sn+2Li_2O$ (7)

While B peak was the result of forming a solid electrolyte interface (SEI) film on $Li_7Ti_5O_{12}$ (Formed from reaction Ⅳ/Ⅳ') [31]. The reaction process of (7)→(4)→(5)→(6) was the decomposition of equation (1). The reactions of Ⅰ/Ⅰ', Ⅱ/Ⅱ', Ⅲ/Ⅲ' and Ⅳ/Ⅳ' were reversible, while reactions of A peak and the reaction of forming a SEI film (B peak) were irreversible. After initial scan, the peaks of A and B disappeared and the profile of third scan was similar with that of second scan, indicating that the reactions after first scan were reversible. Besides, the peaks of Ⅳ/Ⅳ' fade gradually. Such a phenomenon was universal when $Li_4Ti_5O_{12}$ content was less in the composite [26-31]. The results

concluded from Fig. 6(b) were consistent with Fig. 6(a). In Fig. 6(c), no redox peaks of Ⅳ/Ⅳ' and no B peak were shown because there was only SnO_2 in S-0. The lithiation/delithiation details can be also observed from charged/discharge curves as shown in Fig. 6(d)~(f). In initial discharge, a short plateau of $Li_4Ti_5O_{12}$ was showed in Fig. 6(d) and (f), but no other $Li_4Ti_5O_{12}$ plateau in other curves.

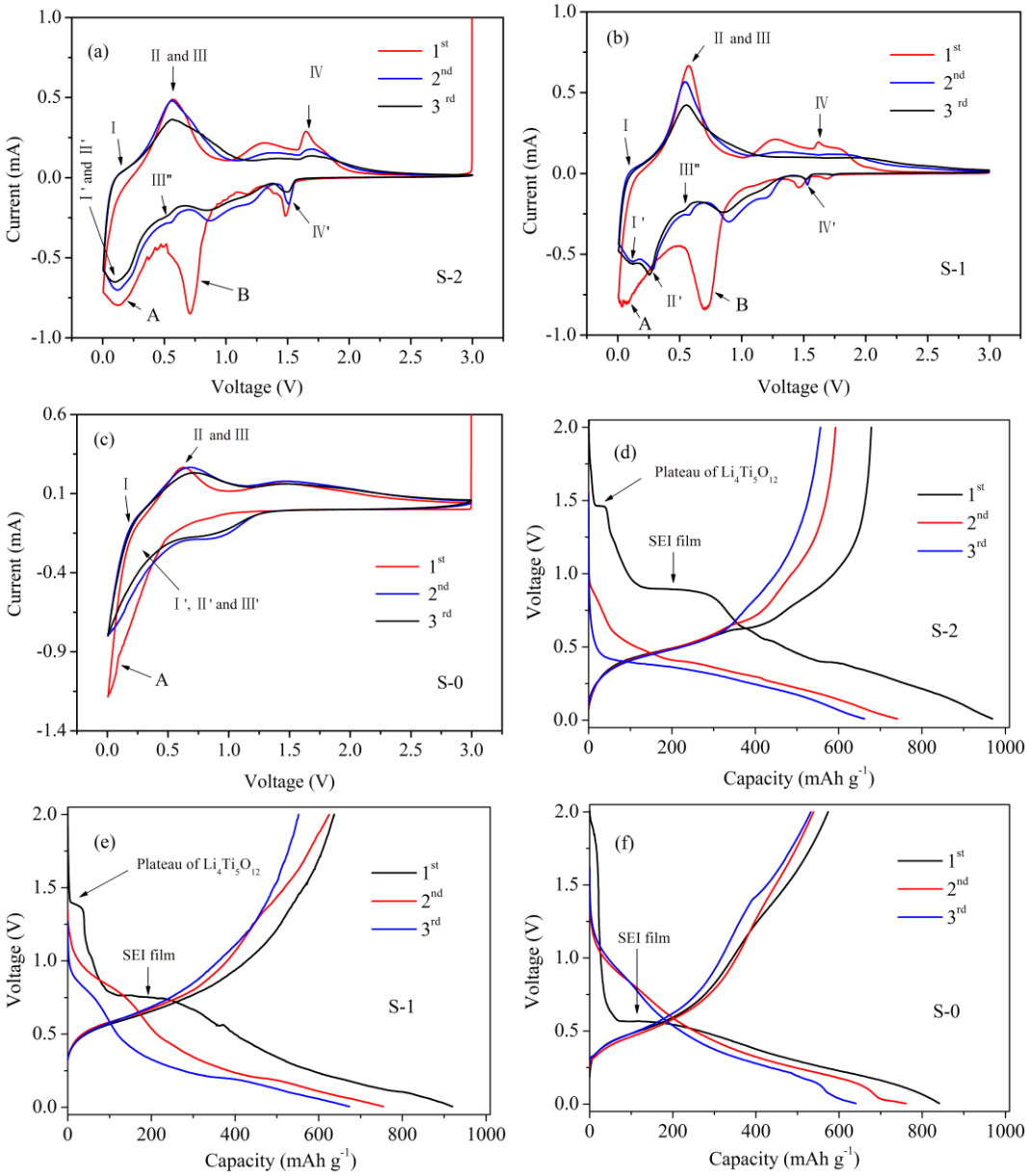

Figure 6. CVs of S-2 (a), S-1 (b) and S-0 (c), charged/discharged curvy of S-2 (d), S-1 (e) and S-0 (f)

Furthermore, a plateau located at ~0.88V for S-2, ~0.75V for S-1 and ~0.57V for S-0 was also observed in initial discharge curve. Those plateaus were owing to form a SEI film. The results of initial charge-discharge curve were consistent with the results of initial CV scan.

4. CONCLUSIONS

$Li_4Ti_5O_{12}$ coated M-SnO_2 was synthesized via sol-gel, hydro-thermal method and high temperature solid-state methods. The particle size of M-SnO_2 was ~1.5 μm, and the thickness of $Li_4Ti_5O_{12}$ coating layer was 60~90 nm. The $Li_4Ti_5O_{12}$ layer acted as Li^+ conductor and volume expansion/contraction buffer layer for SnO_2 anode. The Li^+ diffusion coefficient of S-2 reached to 1.82×10^{-12} cm^2 s^{-1} compared to 6.36×10^{-13} of S-0. At 50 mA g^{-1}, the capacity of S-2 and S-1 was 127.8% and 56.1% higher than that of S-0 after 100^{th} cycle. Moreover, the cyclability and rate cycle performance of SnO_2 anode were improved obviously. The results of the research can be applied for preparing other lithium ion anodes, such as $Li_4Ti_5O_{12}$ coated Fe_2O_3, Co_3O_4, NiO, etc.

ACKNOWLEDGEMENTS
This work was supported by the Undergraduate Research Project of Chongqing University of Technology (No. KLA15025), the National Natural Science Foundation of China (No. 21206203), the Scientific Research Innovation Team of Chongqing University of Technology (No. cqut2015srim) and the Science and Technology Research Program of Chongqing Municipal Education Commission (Grant No. KJ1709217).

References

1. Z. W. Chen, D. Y. Pan, Z. Li, Z. Jiao, M. H. Wu, C. H. Shek, C. M. L. Wu and J. K. L. Lia, *Chem. Rev.*, 114 (2014) 7442.
2. H. K. Wang and A. L. Rogach, *Chem. Mater.*, 26 (2013) 123.
3. S. Böhme, B. Philippe, K. Edström and L. Nyholm, *J. Phys. Chem.* C, 121 (2017) 4924.
4. B. Huang, X. H. Li, Y. Pei, S. Li, X. Cao, R. C. Massé and G. Z. Cao, *Small*, 14 (2016) 1945.
5. J. Xie, N. Imanishi, A. Hirano, Y. Takeda, O. Yamamoto, X. B. Zhao and G. S. Cao, *Solid State Ionics*, 181 (2010) 1611.
6. F. Zhang and L. M. Qi, *Advanced Science*, 3 (2016) 1600049.
7. Lu Li, L. Y. Zhang, F. Chai, T. T. Wang, Z. L. Li, H. M. Xie, C. G. Wang and Z. M. Su, *Eur. J. Inorg. Chem.*, 2016 (2016) 812.
8. Z. Shen, Y. Hu, Y. L. Chen, R. Z. Chen, X. He, X. W. Zhang, H. F. Shao and Y. Zhang, *Electrochim. Acta*, 188 (2016) 661.
9. Y. M. Hu, Q. R. Yang, J. M. Ma, S. L. Chou, M. Y. Zhu and Y. Li, *Electrochim. Acta*, 186 (2015) 271.
10. Y. F. Deng, C. C. Fang and G. H. Chen, *J. Power Sources*, 304 (2016) 81.
11. C. V. Subban, G. Rousse, R. N. Vannier, C. L. Robert, P. Barboux and J. M. Tarascon, *Solid State Ionics*, 283 (2015) 68.
12. C. Muhle, R. E. Dinnebier, L. Wu1llen, G. Schwering and M. Jansen, *Inorganic chemistry*, 43 (2004) 874.
13. M. Wilkening, V. Epp, A. Feldhoff and P. Heitjans, *J. Phys. Chem.* C, 112 (2008) 9291.
14. M. Asano, Y. Kato, T. Harada and Y. Mizutani, *J. Nucl. Mater.*, 2 (1996) 110.
    Q. J. Guo, Q. Wang, G. Chen, Q. X. Shen and B. Li, *RSC Adv.*, 6 (2016) 110032.
15. Y. J. Bai, C. Gong, Y. X. Qi, N. Luna and J. Feng, *J. Mater. Chem.*, 22 (2012) 19054.
16. Y. J. Bai, C. Gong, N. Lun and Y. X. Qi, *J. Mater. Chem. A*, 1 (2013) 89.
17. J. Sugiyama, H. Nozaki, I. Umegaki, K. Mukai, K. Miwa, S. Shiraki, T. Hitosugi, A. Suter, T. Prokscha, Z. Salman, J. S. Lord and M. Mansson, *J. Power Sources*, 304 (2016) 81.
18. X. B. H, Y. L. Zhang, T. B. Zeng, D. J. Zhong, D. W. Zhou and M. Zhang, *Ionics*, 12 (2015) 3289.
19. S. Y. Han, I. Y. Kim, S. H. Lee and S. J. Hwang, *Electrochim. Acta.*, 74 (2012) 59.

20. Y. J. Hao, Q. Y. Lai, Y. D. Chen, J. Z. Lu and X. Y. Ji, *J. Alloy. Compd.*, 1-2 (2008) 404.
21. Y. Y. Wang, Y. J. Hao, Q. Y. Lai, J. Z. Lu, Y. D. Chen and X. Y. Ji, *Ionics*, 1 (2008) 85.
22. X. K. Huang, S. H. Cui, J. B. Chang, P. B. Hallac, C. R. Fell, Y. T. Luo, B. Metz, J. W. Jiang, P. T. Hurley and J. H. Chen, *Angew. Chem.*, 127 (2015) 1510.
23. J. Shu, L. Hou, R. Ma, M. Shui, L. Y. Shao, D. J. Wang, Y. L. Ren and W. D. Zheng, *RSC Adv.*, 2 (2012) 10306.
24. P. C. Tsai, W. D. Hsu and S. K. Lin, *J. Electrochem. Soc.*,161 (2014) A439.
25. R.Nasiraei, M. R. Fadavieslam and H. A. Juybari, *Pramana*, 87 (2016) 30.
26. C. J. Liu, F. H. Xue, H. Huang, X. H. Yu, C. J. Xie, M. H. Shi, G. Z. Cao, Y. G. Jung and X. L. Dong, *Electrochim. Acta*, 129 (2014) 93.
27. L. Huang, J. S. Cai, Y. He, F. S. Ke and S. G. Sun, *Electrochem. Commun.*, 11 (2009) 950.
28. J. D. Yana, H. H. Song, H. J. Zhang, J. Y. Yan, X. H. Chen, F. Wang, H. Y. Yang and M. B. Gomic, *Electrochim. Acta*, 72 (2012) 186.
29. G. Wang, Y. Q. Ma, Z. Y. Liu and J. N. Wu, *Electrochim. Acta*, 65 (2012) 275.
30. Z. X. Chen, Y. L. Cao, J. F. Qian, X. P. Ai and H. X. Yang, *J. Mater. Chem.*, 20 (2010) 7266.
31. C. M. Wang, W. Xu, J. Liu, J. G. Zhang, L. V. Saraf, B. W. Arey, D. Choi, Z. G. Yang, J. Xiao, S. Thevuthasan and D. R. Baer, *Electrochim. Acta*, 186 (2015) 271.
32. S. Wang, K. Yang, F. Gao, D. Y. Wang and C. Shen, *RSC Adv.*, 6 (2016) 77105.